iScience

CellPress
OPEN ACCESS

Article

Perovskite-based photodetector for real-time and quantitative monitoring of sports motion

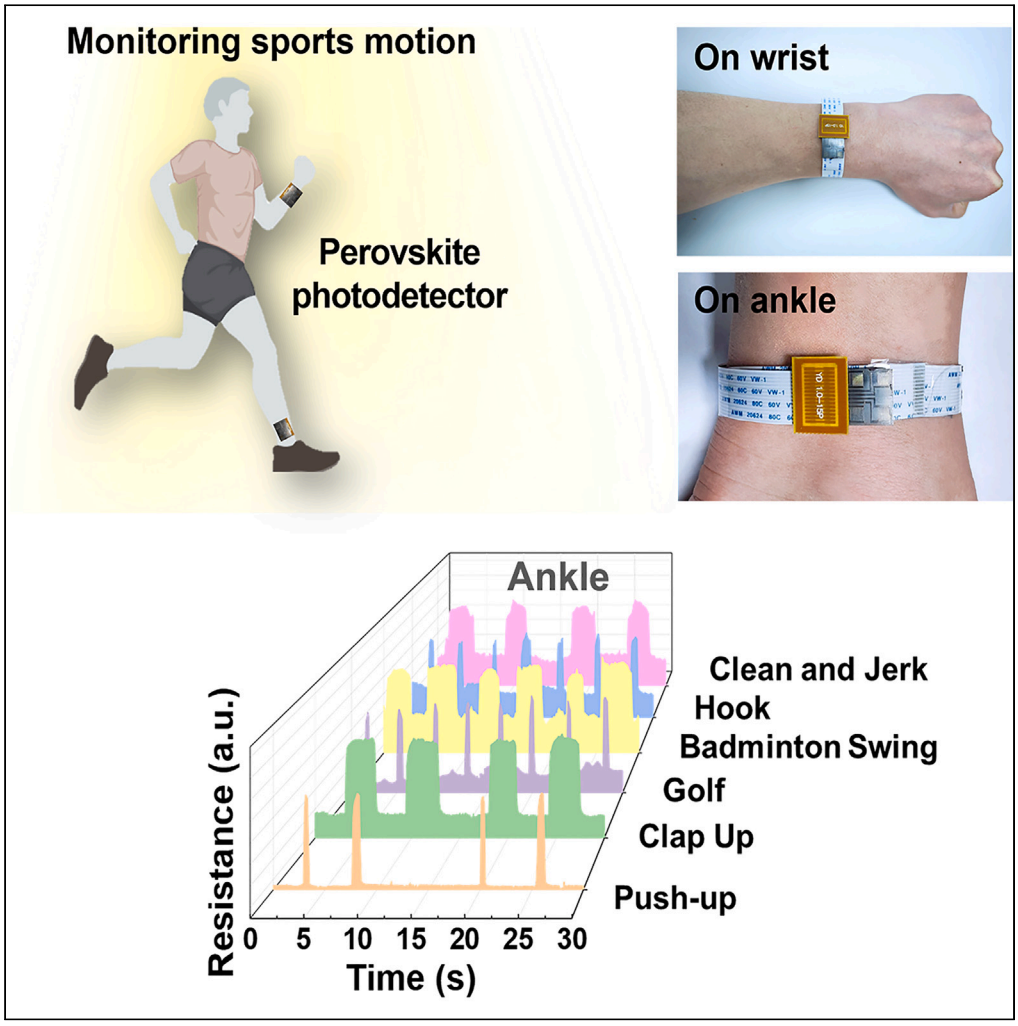

Yuming Hu, Tingqing Wu, Jiabing Zhang, ..., Chunbao Li, Meng Su, Yanlin Song

cli301@foxmail.com (C.L.)
sumeng1988@iccas.ac.cn (M.S.)
ylsong@iccas.ac.cn (Y.S.)

Highlights

A wearable perovskite photodetector is successfully constructed

-SH and -CONH- groups are introduced to passivate uncoordinated Pb^{2+}

A real-time and quantitative monitoring motion method is presented

Hu et al., iScience 26, 108298
November 17, 2023 © 2023
https://doi.org/10.1016/j.isci.2023.108298

iScience

CellPress
OPEN ACCESS

Article

Perovskite-based photodetector for real-time and quantitative monitoring of sports motion

Yuming Hu,[1,2,8] Tingqing Wu,[1,2,8] Jiabing Zhang,[3] Wei Sun,[4] Mengfei Lv,[5] Hongfei Xie,[1,2] Tangyue Xue,[6] Teng Han,[4] Chunbao Li,[7,*] Meng Su,[1,2,9,*] and Yanlin Song[1,2,*]

SUMMARY

Reliable monitoring the movement amplitude and dynamics during sports exercise is significant for improving training results and preventing training wound. Here, we present a printed perovskite-based photodetector for real-time and quantitative monitoring of sports motion. The ordered nucleation and growth of perovskite crystals are regulated by the 4-acetamidothiophenol (AMTP) at the interface, which promotes the size of perovskite crystals into the micrometer. Benefiting from the uniformity of the AMTP-regulated $MAPbI_3$, the as-prepared photodetector gives great photocurrent response under indoor light or outdoor light. During the exercise, real-time monitoring sports motion is achieved through detecting the illumination changing of photodetectors attaching on the wrist and ankles. Moreover, twelve kinds of common sports can be quantitatively analyzed with the detection of illumination changing on the photodetector. Such photodetector provides an efficient measurement method of wearable electronics for sports monitoring.

INTRODUCTION

Tracking and monitoring of whole-body motions during sports have important applications in posture analysis, sport training effect, rehabilitation evaluation, human-computer interaction, and virtual reality.[1–10] Especially after COVID-19, if the body starts high-intensity or high-volume sport exercise too early after infection, important organs such as the heart and lungs will be damaged, and the body may be re-infected with the novel coronavirus. It is significant to monitor the sports motions in daily life. Commonly, high-speed camera is adopted for monitoring sports motions. The key information is analyzed and extracted from a large number of images, which has many disadvantages and limitations. While a large number of photos and videos must be analyzed, higher requirements on computer hardware are essential with huge energy consumption. It is unimaginable for people to use the high-grade camera for analyzing daily sports motions. Recently, wearable sensors have been investigated to monitor sports motions via recording the strain change of skins.[11–15] These strain sensors must be closely adhered on the skin to keep records trusted and accurate, which makes the sporter uncomfortable in training.

Photovoltaic sensors can easily achieve the senseless interaction in multi-dimensional space by transferring the optical signals to electric signals. Compared with traditional contact sensors, the non-contact interaction based on light and shadow of photovoltaic devices can effectively avoid the uncomfortable problem of wearable sensors. The non-contact photovoltaic devices can effectively reduce the risk of pathogen transmission to avoid health and safety concerns. Recently, metal halide perovskite has been widely used in photovoltaic device due to its low manufacturing cost, wide optical absorption range, adjustable band gap, and high carrier mobility.[16–29] With the continuous improvement of the performance of perovskite photovoltaic devices, more and more research has paid attention to the field of wearable devices.[11–13] Thus, it is feasible to achieve real-time and quantitative monitoring of sports motion via recording the illumination change around the sporter via the photodetectors. However, it remains a challenge to obtain high-quality, stable perovskite crystals, which limits its practical application in photovoltaic devices. What's worse, some organic volatile components inevitably escape from perovskite polycrystalline films during thermal annealing. Part of Pb^{2+} is dissociated in the grain boundaries and surfaces of perovskite films, resulting in the degradation of device performance. Therefore, different methods (such as crystal regulation, surface passivation, interface modification, etc.) have been proposed to reduce the density of defect states in perovskite polycrystalline films.[30–43] However, perovskite polycrystalline films with low defect density

[1]Key Laboratory of Green Printing, CAS Research/Education Center for Excellence in Molecular Sciences, Institute of Chemistry, Chinese Academy of Sciences (ICCAS), Beijing Engineering Research Center of Nanomaterials for Green Printing Technology, Beijing National Laboratory for Molecular Sciences (BNLMS)
[2]School of Chemical Science, University of Chinese Academy of Sciences, Beijing 100049, P.R. China
[3]Graduate School of Medical School of Chinese PLA Hospital, Beijing 100853, P.R. China
[4]Institute of Software, Chinese Academy of Sciences, Beijing 100049, P.R. China
[5]Faculty of Information Technology, Beijing University of Technology, Beijing 100124, P.R. China
[6]School of Materials Science and Engineering, Zhengzhou University, Zhengzhou 450001, P.R. China
[7]Department of Orthopaedic Medicine, Fourth Medical Center, PLA General Hospital, Beijing 100853, P.R. China
[8]These authors contributed equally
[9]Lead contact
*Correspondence: cli301@foxmail.com (C.L.), sumeng1988@iccas.ac.cn (M.S.), ylsong@iccas.ac.cn (Y.S.)
https://doi.org/10.1016/j.isci.2023.108298

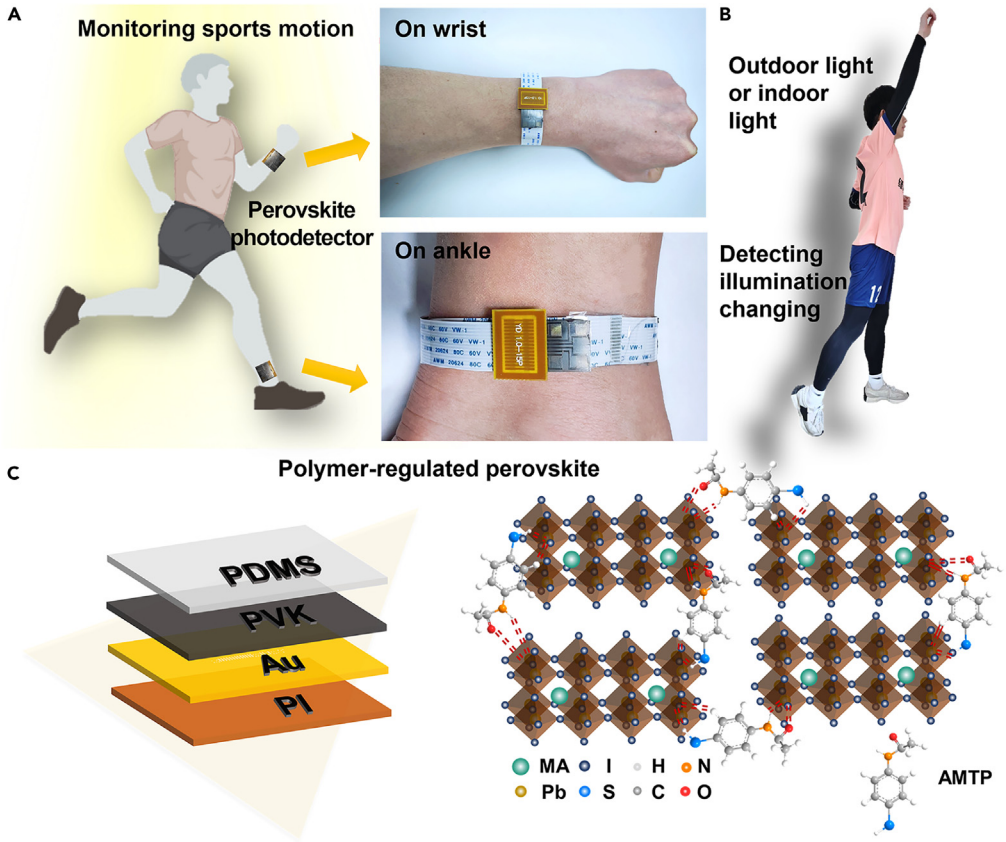

Figure 1. Design of wearable perovskite-based photodetector for real-time and quantitative monitoring of sports motion

(A) Schematic illustration of the perovskite-based photodetector attached on the wrist (upper right) or ankle (lower right) for motion monitoring.

(B) Perovskite-based photodetector can detect the illumination changing caused by actions under outdoor light or indoor light.

(C) Structure diagram of the polymer-regulated perovskite photodetector.

at micron scale are still difficult to be prepared. High density of defect state will result in low photocurrent of perovskite film under indoor light, which limits its performance in portable illumination monitoring.[44–46]

Herein, we present a polymer-regulated perovskite photodetector for real-time and quantitative monitoring of sports motion. During the crystallization process of perovskite, 4-acetamidothiophenol (AMTP) molecules will provide sites for homogeneous nucleation and assist the formation of large grains. Moreover, AMTP molecules are demonstrated in the degradation of grain boundaries and the enhancement of carrier mass in perovskite films. The AMTP-regulated perovskite photodetector gives photocurrent response under indoor light or outdoor light. During the exercise, real-time monitoring sports motion is achieved through detecting the illumination changing of photodetectors. Accordingly, twelve kinds of common sports can be quantitatively analyzed with the detection of illumination changing on the photodetector. Such photodetector provides a novel measurement method of wearable electronics for sports monitoring.

RESULT AND DISCUSSION

Design of wearable $MAPbI_3$-based photodetector for real-time and quantitative monitoring of sports motion

Figure 1 schematically demonstrates the application and structure design of wearable perovskite-based photodetector. Figure 1A shows the application scenario of perovskite-based wearable photodetector. The perovskite-based photodetectors are attached on the wrist or ankle. Due to the difference in the amplitude of limb oscillation during sports exercise, the illumination changes in the relative position of the detector, which leads to the corresponding resistance response of photodetector. We exploit the excellent photoelectric response of the perovskite material to realize real-time and quantitative motion monitoring of sports motion. When the detecting illumination intensity changes from strong light (outdoor light) to weak light (indoor light), the motion monitoring can still be achieved (Figure 1B). Figure 1C demonstrates the structure of a perovskite-based photodetector for sports motion monitoring. The patterned gold electrodes are deposited on the pre-stretched polyimide (PI) substrate. The perovskite photoactive layer is spin-coated on the aforementioned substrate by using the $MAPbI_3$ precursor solution modulated with 4-acetamidothiophenol (AMTP) molecules. During the crystallization and nucleation of $MAPbI_3$ wet films, -SH and -CONH- groups in AMTP molecules can be paired with uncoordinated Pb^{2+} to form complexes, which can effectively reduce the defect

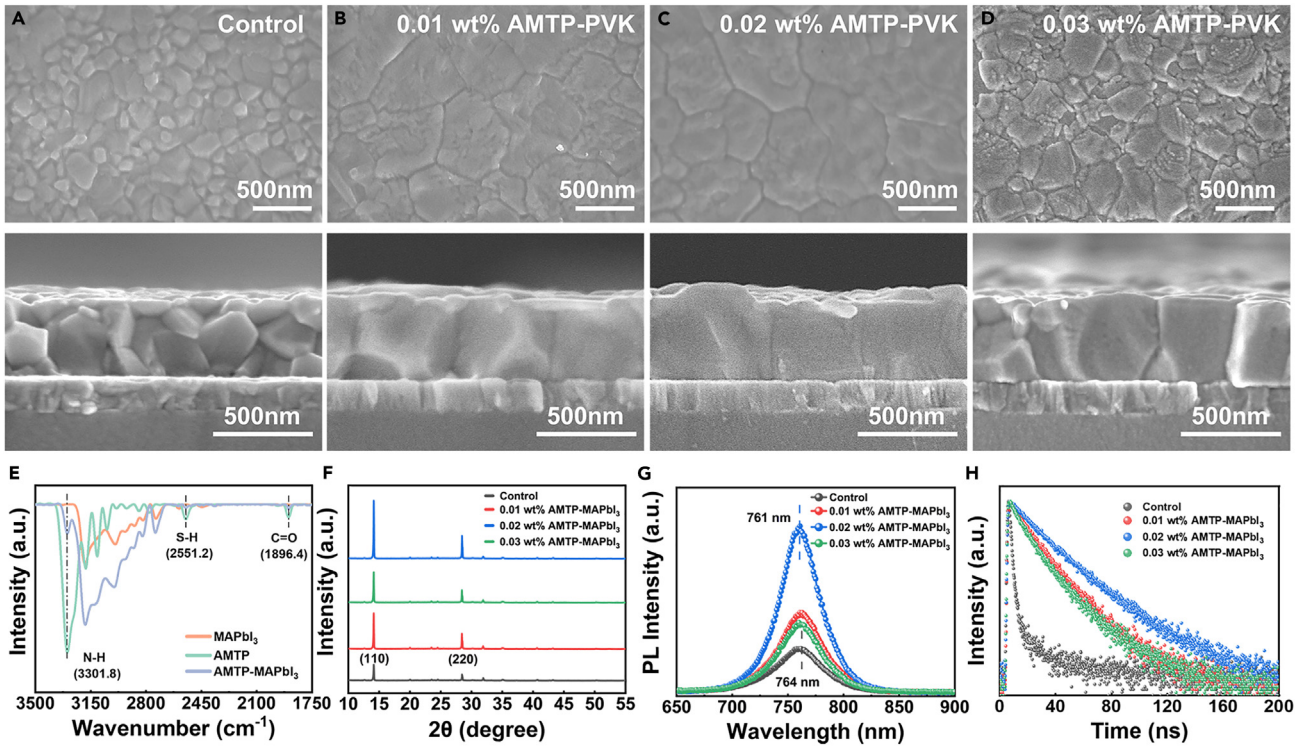

Figure 2. Characterization of crystallinity and optical properties of AMTP-regulated $MAPbI_3$

(A) Surface and cross-sectional SEM images of the $MAPbI_3$ films. Scale bars, 500 nm.

(B) Surface and cross-sectional morphologies SEM images of the 0.01wt % AMTP-$MAPbI_3$ films. Scale bars, 500 nm.

(C) Surface and cross-sectional morphologies SEM images of the 0.02wt % AMTP-$MAPbI_3$ films. Scale bars, 500 nm.

(D) Surface and cross-sectional morphologies SEM images of the 0.03 wt % AMTP-MAPbI3 films. Scale bars, 500 nm.

(E) Fourier transform infrared spectra of $MAPbI_3$, AMTP and AMTP-$MAPbI_3$.

(F) XRD characterization of $MAPbI_3$ and AMTP-$MAPbI_3$ films with different doping concentrations.

(G) PL characterization of $MAPbI_3$ and AMTP-$MAPbI_3$ films with different doping concentrations.

(H) TRPL characterization of $MAPbI_3$ and AMTP-$MAPbI_3$ films with different doping concentrations.

density on the surface and grain boundary of the $MAPbI_3$ film. Compared with the nucleation rate of the control $MAPbI_3$-DMSO complexes, AMTP-based complexes have a faster nucleation supersaturation rate. This can achieve rapid nucleation and promote the formation of large perovskite grains. Thus, the preparation of perovskite-based photodetector is completed (left). A schematic diagram of perovskite crystallization induced by molecule AMTP is shown on the right.

Characterization of crystal morphologies and optical properties

In order to investigate the effect of AMTP molecules on perovskite, we prepare the $MAPbI_3$ film (Control) and 4-acetamidothiophenol-doped perovskite films (AMTP-$MAPbI_3$) with different concentrations of AMTP molecules. Figures 2A–2D show the surface and cross-sectional morphologies of scanning electron microscopy (SEM) images at four different proportions. It is found that the control sample presents the small grain size. Correspondingly, multilayer grain arrangement occurred at the vertical growth interface (Figure 2A). When 0.01wt % AMTP was added, the grain size increased significantly. At the same time, the vertical grain growth also changed from multilayer to single layer. It is attributed to the special groups of -CONH- and -SH groups in AMTP molecules. Both -CONH- and -SH groups in AMTP molecules can coordinate with uncoordinated Pb^{2+} to form complexes, which effectively reduce the defect density in $MAPbI_3$ and provide conditions for the growth of large grains. When the concentration of AMTP was increased to 0.02wt %, the grain size of perovskite further increased (>1 μm) (Figure 2C). It can be seen from Figure S11 that 0.02wt % AMTP-$MAPbI_3$ films with larger $MAPbI_3$ grain size have lower surface roughness than the control film. Compared with the addition of 0.01wt % AMTP molecules, the transverse grain size is more uniform, and the binding at the grain boundary is closer, and the consistent morphology is displayed at the cross section. When the concentration of AMTP molecules increased to 0.03wt %, the grain size of $MAPbI_3$ decreased significantly, the local defects increased significantly, and the longitudinal crystallization also showed a trend from single layer to multilayer (Figure 2D). This phenomenon indicates that the addition of AMTP can effectively reduce the defect density in $MAPbI_3$, increase the grain size and improve the uniformity of the film at an appropriate concentration range. However, when the AMTP above a critical concentration was added, excessive AMTP molecules accumulated in $MAPbI_3$ as impurities, affecting the ordered growth of crystals. Figure S6 shows the thickness comparison between 0.02wt % AMTP-$MAPbI_3$ film and the control.

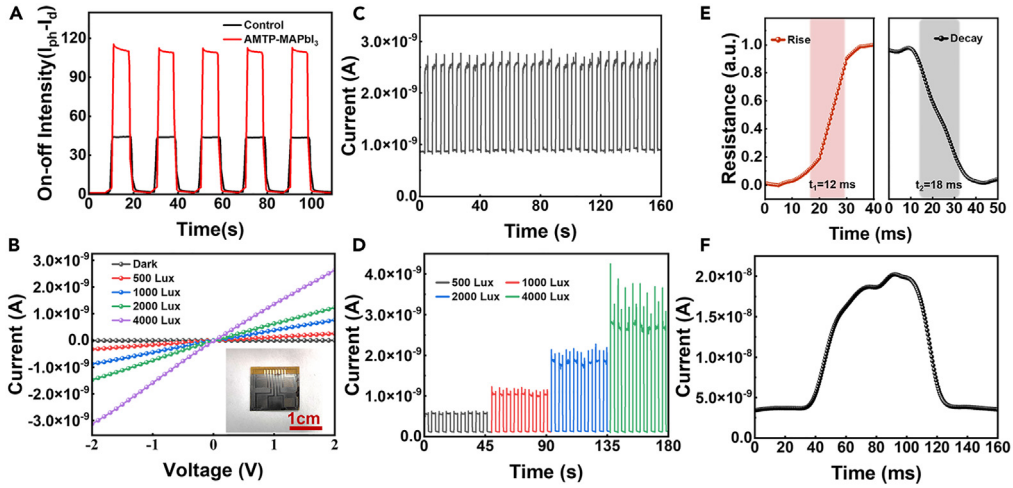

Figure 3. Characterization of optoelectronic performances of the AMTP-$MAPbI_3$ based photodetectors

(A) I-T response of the control and AMTP- $MAPbI_3$ based photodetectors in the dark condition and under 500 Lux light illumination.

(B) I-V curves of the AMTP-$MAPbI_3$ based photodetector in the dark condition and under different (500, 1000, 2000, 4000 Lux) illuminance. The inset shows an as-prepared AMTP- $MAPbI_3$ photodetector. Scale bars, 1 cm.

(C) Current response of AMTP-$MAPbI_3$ based photodetectors at 30 consecutive switches.

(D) Current response of AMTP-$MAPbI_3$ based photosensors under different (500, 1000, 2000, 4000 Lux) illumination.

(E) Response time and decay time of the AMTP-$MAPbI_3$ based photosensors.

(F) Current response of the AMTP based photodetector during a quick sport motion.

In order to further explore the influence of AMTP on the crystal structure of $MAPbI_3$, we also conducted a series of characterization. Figure 2E shows the Fourier transform infrared spectral (FTIR) characterization of $MAPbI_3$, AMTP molecules, and 0.02wt % AMTP-doped $MAPbI_3$. N-H, S-H, and C=O groups stretching vibration peaks located at 3301.8 cm^{-1}, 2551.2 cm^{-1} and 1896.4 cm^{-1} on AMTP could also be found on AMTP-$MAPbI_3$, while they were not found in $MAPbI_3$. AMTP molecules have been successfully involved in the formation of perovskite films. To illustrate the effect of AMTP on crystal morphology, Figure 2F shows the XRD characterization of perovskite films doped with four different concentrations of AMTP molecules. The perovskite film doped with AMTP had higher and sharper (110) and (220) diffraction peaks, indicating its role in improving crystallinity and adjusting grain size. In addition, the doping concentration of 0.02wt % exhibited the highest diffraction peak, while the diffraction peak of 0.03wt % was lower than that of 0.01wt %. The results were consistent with SEM characterization, and 0.02wt % was determined to be the most appropriate doping concentration. Furthermore, photoluminescence (PL) and time-resolved photoluminescence (TRPL) were performed (Figures 2G and 2H). AMTP-$MAPbI_3$ showed a stronger PL peak than the control, and the emission peak of AMTP-$MAPbI_3$ blueshifted by 3 nm (Figure 2G). In previous studies, it was found that spontaneous recombination between trap states would lead to the redshift of emission peak, while passivation of trap states would lead to the blueshift of emission peak.[10] The interaction between AMTP and $MAPbI_3$ passivated the defects at grain boundaries and reduced the non-radiative recombination of carriers. This passivation was achieved by the S atoms occupying the vacancy I in AMTP molecules to form a more tightly bonded Pb-S lattice structure. Thus, the photogenerated carrier lifetime of $MAPbI_3$ increased from 14.06 ns to 32.32 ns (Figure 2H), which further confirmed the role of AMTP molecules in the degradation of grain boundaries and the enhancement of carrier lifetime in $MAPbI_3$ films. Details of the TRPL characterization of $MAPbI_3$ and AMTP-$MAPbI_3$ films with different doping concentrations are supplemented in Table S1.

Characterization of optoelectronic performances of the AMTP-$MAPbI_3$ based photosensors

In order to verify the photoelectric properties of $MAPbI_3$ films regulated by AMTP molecule, photodetectors with PI/AMTP-$MAPbI_3$ planar structure were prepared successfully. Under continuous indoor light irradiation (light intensity about 500 Lux), the control and AMTP-$MAPbI_3$ based photoelectric detection were covered for 10 s at an interval of 20 s, to compare the influence of AMTP molecule on the switch response (Figure 3A). It can be found that the AMTP- $MAPbI_3$ based photodetector displayed about 110 times the ratio of light to dark current, while the control only showed about 40 times. AMTP-$MAPbI_3$ based photodetectors have better light response. Figure 3B shows the current response of AMTP-$MAPbI_3$ based photodetectors under dark light and different illuminance (500, 1000, 2000, and 4000 Lux). AMTP-$MAPbI_3$ based photodetectors displayed outstanding current response under indoor light (about 500 Lux) and outdoor light (about 4000 Lux). In dark environment, the AMTP-$MAPbI_3$ photodetector exhibits an excellent dark current response of 2.5×10^{12} (Figure S8). At the same time, with the increase of illumination intensity, the response current also raised accordingly, which laid a good foundation for the subsequent sports motion monitoring. Further testing found that the AMTP-$MAPbI_3$ photodetector showed a high responsivity of 6.01 A/W at 450 nm laser with a detectivity of 1.60×10^{13} Jones (Figure S9). The inset shows an as-prepared AMTP-$MAPbI_3$ photodetector, which consists of four finger areas and sends electrical signals through an electrode path at the bottom. The AMTP-$MAPbI_3$ based photodetector was connected to a computer to

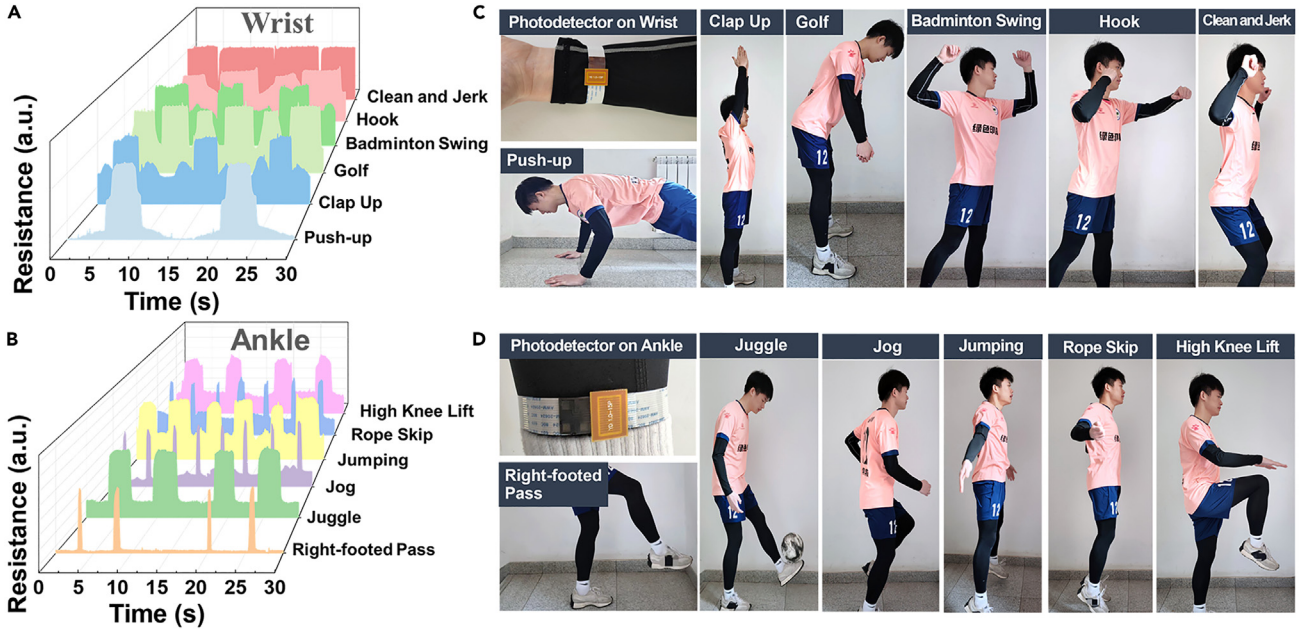

Figure 4. Real-time and quantitative motion monitoring based on AMTP-MAPbI$_3$ photodetector The distinct electronic signals of two positions and twelve sports motions

(A) The real-time monitoring of resistance changes of six kinds of sports motion of the same position (wrist).

(B) The real-time monitoring of resistance changes of six kinds of sports motion of the same position (ankle).

(C) Photos of AMTP-MAPbI$_3$ based photodetector attached at the wrist and photographs of six kinds of sports motion.

(D) Photos of AMTP-MAPbI$_3$ based photodetector attached at the ankle and photographs of six kinds of sports motion.

further verify its interactive capabilities, and a Python program was developed to continuously capture and analyze the sensor data stream. Figure 3C shows the current response changes of the AMTP-MAPbI$_3$ based photodetector during 30 times of occlusion and irradiation at the light intensity of 500 Lux. Figure S10 shows the on-off intensity of the AMTP-MAPbI$_3$ photodetector after 300 consecutive switches at the light intensity of 500 Lux. The AMTP-MAPbI$_3$ based photodetector demonstrated satisfied stability in recognizing continuous motion, as shown by the smooth change of low resistance when irradiated and high resistance when blocked. Figure 3D shows the current response of the AMTP-MAPbI$_3$ based photodetector when the ambient light changes from 500 Lux to 4000 Lux in the process of continuous occlusion and irradiation. The current response of AMTP-MAPbI$_3$ based photodetectors is similar in response to the same action and under the same ambient light condition. With the increase of external light intensity, the variation of current of AMTP-MAPbI$_3$ based photodetector also increased. This indicates that the AMTP-MAPbI$_3$ based photodetector can sense the changes of irradiated light, and has the basis of quantitative motion recognition. Figure S7 further shows that after 500 bends with a curvature radius of 7 mm, the performance of the MAPbI$_3$ photodetector decayed almost completely, while the current response of AMTP-MAPbI$_3$ photodetector remained above 91% of its initial state. Figure 3E shows the response time and attenuation time of the AMTP-MAPbI$_3$ based photodetector when it faces motion recognition. When a quick gesture was made, the resistance response rose rapidly within 12 ms and fell rapidly within 18 ms. Movements with a completion time of more than 80 ms can be successfully recognized by the AMTP-MAPbI$_3$ based photodetector when performing a continuous gesture wave (Figure 3F). The fast response capability of the detector was demonstrated with different frequency gestures from low speed to high speed (Video S1). Such recognition speed can match almost all the movements of the human body, and real-time motion monitoring can be achieved.

Real-time and quantitative motion monitoring based on AMTP-MAPbI$_3$ based photodetector

To demonstrate real-time, quantitative motion monitoring, the AMTP-MAPbI$_3$ based photodetectors were attached on one's wrist and ankle to analyze resistance responses to twelve common motions. A white light source is fixed 1.5 m away, and the illumination on the photodetector was 500 Lux by controlling the intensity of the light source. The AMTP- MAPbI$_3$ based photodetector on the wrist was used to monitor changes in electrical resistance during six different actions (push-up, clap up, golf, badminton swing, hook, clean, and jerk) (Figures 4A and 4C). The relative position of the AMTP-MAPbI$_3$ based photodetector at the wrist will also change due to the different amplitude, speed, and angle of the arm raised under different motions. When the relative position of the AMTP-MAPbI$_3$ based photodetector changes, the light and shadow information perceived by the detector will also change, so as to output a section of resistance response with characteristic information in real time. The corresponding resistance response can then be recorded through continuous action input. Accordingly, the motion state can also be identified by the specific resistance response waveform. Because the

change of action frequency does not affect the waveform of resistance response, it only changes the frequency of resistance response peak. Therefore, the real-time and quantitative monitoring of motion attitude can be attached based on the rapid response of resistance. As another demonstration, the AMTP-$MAPbI_3$ based photodetector on the ankle was also investigated to monitor different actions (right-footed pass, juggle, jog, jumping rope skip, high knee lift) (Figures 4B and 4D). Four other actions and their resistive responses are also shown (Figures S1–S4). The photodetector can produce different characteristic resistance response peaks for different motions. For similarly expressed motion, AMTP-$MAPbI_3$ can show significantly different characteristic resistance responses based on different motion frequencies, intervals, and limb amplitudes (Figures S3 and S5). The overall shape of the response peaks is significantly different due to the special light and shadow information generated by the ankle. This way of changing the wearing position can effectively broaden the application scenarios of the AMTP-$MAPbI_3$ based photodetectors and improve the detection capability.

Conclusion

In conclusion, we have demonstrated the sports motion monitoring strategy via the detection of illumination changing around the sporter. A photodetector response to the changing of indoor light or outdoor light is achieved via the uniform polymer-regulated perovskite crystal. We have experimentally optimized the doping content of AMTP at the interface to reduce the defect density and improve the size of perovskite crystals. After investigating the photoresponse ability of an as-prepared photodetector, the photocurrent can reach 3.27×10^{-10} An under indoor ambient light of about 500 Lux, and corresponding on-off ratio exceeds 114 times. We also show proof-of-concept monitoring of sports motion via detecting the illumination changing around the photodetector on the sporter and demonstrate the capabilities of accurate analysis of common sports. This photodetector provides a novel measurement platform of wearable electronics for sports monitoring, which demonstrates an idea for creating future robots' sense of touch and perception of surrounding environmental risks.

Limitations of the study

Except for photodetectors, the data processing and communication electronics must be integrated with the battery as one part to achieve the wearable applications. Benefiting from their excellent photoelectric characteristics, perovskite-based solar cells have attracted great attention. In the future, all-in-one perovskite-based wearable devices can be further investigated to monitor sports motions without batteries.

STAR★METHODS

Detailed methods are provided in the online version of this paper and include the following:

- KEY RESOURCES TABLE
- RESOURCE AVAILABILITY
  - Lead contact
  - Materials availability
  - Data and code availability
- EXPERIMENTAL MODEL AND SUBJECT DETAILS
- METHOD DETAILS
  - Experimental procedures

SUPPLEMENTAL INFORMATION

Supplemental information can be found online at https://doi.org/10.1016/j.isci.2023.108298.

ACKNOWLEDGMENTS

This work thanks for the financial support from Beijing Nova Program from Beijing Municipal Science & Technology Commission (Grant No. Z201100006820037, Z211100002121001), National Nature Science Foundation of China (Grant No. 52222313, 22075296, 91963212), Youth Innovation Promotion Association CAS (No. 2020032), Beijing National Laboratory for Molecular Sciences (No. BNLMS-CXXM-202005).

AUTHOR CONTRIBUTIONS

H.Y., W.T. S. M., and S.Y. conceived and designed the experiments. H.Y. and W.T. prepared materials, performed the experiments, and analyzed experimental data. H.T., S.W., and L.M. assisted complete the test. Z.J., L.C., X.H., and X.T. provided suggestions. H.Y. and W.T wrote the manuscript, S.M. revised the manuscript. S.M. and S.Y. supervised all the aspects of this work and provided financial support. All authors discussed the results and contributed to the paper.

DECLARATION OF INTERESTS

The authors declare no competing interests.

Received: April 4, 2023
Revised: July 4, 2023
Accepted: October 19, 2023
Published: October 27, 2023

REFERENCES

1. Yin, R., Wang, D., Zhao, S., Lou, Z., and Shen, G. (2020). Wearable Sensors Enabled Human–Machine Interaction Systems: From Design to Application. Adv. Funct. Mater. *31*, 2008936.
2. Liu, F., Liu, K., Rafique, S., Xu, Z., Niu, W., Li, X., Wang, Y., Deng, L., Wang, J., Yue, X., et al. (2023). Highly Efficient and Stable Self-Powered Mixed Tin-Lead Perovskite Photodetector Used in Remote Wearable Health Monitoring Technology. Adv. Sci. *10*, e2205879.
3. Polat, E.O., Mercier, G., Nikitskiy, I., Puma, E., Galan, T., Gupta, S., Montagut, M., Piqueras, J.J., Bouwens, M., Durduran, T., et al. (2019). Flexible graphene photodetectors for wearable fitness monitoring. Sci. Adv. *5*, eaaw7846.
4. Park, T., Kim, D., Shin, B., Hur, J., and Yoo, H. (2022). Facile, Real Time Identification of Blood Components with Self Powered Organic–Inorganic Heterostructure Photodetectors. Adv. Opt. Mater. *10*, 2102542.
5. Wang, L., Lou, Z., Jiang, K., and Shen, G. (2019). Bio Multifunctional Smart Wearable Sensors for Medical Devices. Adv. Intell. Syst. *1*, 1900040.
6. Li, J., Wang, Y., Liu, L., Xu, S., Liu, Y., Leng, J., and Cai, S. (2019). A Biomimetic Soft Lens Controlled by Electrooculographic Signal. Adv. Funct. Mater. *29*, 1903762.
7. Yu, X., Xie, Z., Yu, Y., Lee, J., Vazquez-Guardado, A., Luan, H., Ruban, J., Ning, X., Akhtar, A., Li, D., et al. (2019). Skin-integrated wireless haptic interfaces for virtual and augmented reality. Nature *575*, 473–479.
8. Zhang, Z., Wen, F., Sun, Z., Guo, X., He, T., and Lee, C. (2022). Artificial Intelligence Enabled Sensing Technologies in the 5G/Internet of Things Era: From Virtual Reality/Augmented Reality to the Digital Twin. Adv. Intell. Syst. *4*, 2100228.
9. Gao, Z., Zhou, H., Dong, K., Wang, C., Wei, J., Li, Z., Li, J., Liu, Y., Zhao, J., and Fang, G. (2022). Defect Passivation on Lead-Free CsSnI(3) Perovskite Nanowires Enables High-Performance Photodetectors with Ultra-High Stability. Nano-Micro Lett. *14*, 215.
10. Shao, Y., Xiao, Z., Bi, C., Yuan, Y., and Huang, J. (2014). Origin and elimination of photocurrent hysteresis by fullerene passivation in $CH_3NH_3PbI_3$ planar heterojunction solar cells. Nat. Commun. *5*, 5784.
11. Hu, Y., Niu, T., Liu, Y., Zhou, Y., Xia, Y., Ran, C., Wu, Z., Song, L., Müller-Buschbaum, P., Chen, Y., and Huang, W. (2021). Flexible Perovskite Solar Cells with High Power-Per-Weight: Progress, Application, and Perspectives. ACS Energy Lett. *6*, 2917–2943.
12. Hu, X., Li, F., and Song, Y. (2019). Wearable Power Source: A Newfangled Feasibility for Perovskite Photovoltaics. ACS Energy Lett. *4*, 1065–1072.
13. Zhao, R., Gu, Z., Li, P., Zhang, Y., and Song, Y. (2021). Flexible and Wearable Optoelectronic Devices Based on Perovskites. Adv. Mater. Technol. *7*, 2101124.
14. Su, M., and Song, Y. (2022). Printable Smart Materials and Devices: Strategies and Applications. Chem. Rev. *122*, 5144–5164.
15. Wu, T., Huang, Z., Li, L., Sun, W., Xue, T., Pan, Q., Xie, H., Chen, S., Guo, L., Chi, J., et al. (2022). Wearable Perovskite Based Shadow Recognition Sensor for Ambient and Nonobtrusive Human–Computer Interaction. Adv. Intell. Syst. *5*, 220030.
16. Chen, S., Teng, C., Zhang, M., Li, Y., Xie, D., and Shi, G. (2016). A Flexible UV-Vis-NIR Photodetector based on a Perovskite/Conjugated-Polymer Composite. Adv. Mater. *28*, 5969–5974.
17. van Breemen, A.J.J.M., Ollearo, R., Shanmugam, S., Peeters, B., Peters, L.C.J.M., van de Ketterij, R.L., Katsouras, I., Akkerman, H.B., Frijters, C.H., Di Giacomo, F., et al. (2021). A thin and flexible scanner for fingerprints and documents based on metal halide perovskites. Nat. Electron. *4*, 818–826.
18. Wu, W., Han, X., Li, J., Wang, X., Zhang, Y., Huo, Z., Chen, Q., Sun, X., Xu, Z., Tan, Y., et al. (2021). Ultrathin and Conformable Lead Halide Perovskite Photodetector Arrays for Potential Application in Retina-Like Vision Sensing. Adv. Mater. *33*, e2006006.
19. Gu, Z., Huang, Z., Li, C., Li, M., and Song, Y. (2018). A general printing approach for scalable growth of perovskite single-crystal films. Sci. Adv. *4*, eaat2390.
20. Xu, J., Li, X., Chang, H., Zhao, B., Tan, X., Yang, Y., Tian, H., Zhang, S., and Ren, T.L. (2022). Electrooculography and Tactile Perception Collaborative Interface for 3D Human-Machine Interaction. ACS Nano *16*, 6687–6699.
21. Jena, A.K., Kulkarni, A., and Miyasaka, T. (2019). Halide Perovskite Photovoltaics: Background, Status, and Future Prospects. Chem. Rev. *119*, 3036–3103.
22. Li, C., Yang, J., Wang, Y., Qi, Y., Yang, W., and Li, Y. (2020). Advances in perovskite photodetectors. InfoMat *11*, 1247–1256.
23. Hao, D., Zou, J., and Huang, J. (2019). Recent developments in flexible photodetectors based on metal halide perovskite. InfoMat *2*, 139–169.
24. Wang, H., Wang, Y., Xuan, Z., Chen, T., Zhang, J., Hao, X., Wu, L., Constantinou, I., and Zhao, D. (2021). Progress in Perovskite Solar Cells towards Commercialization-A Review. Materials *14*, 6569.
25. Li, L., Ye, S., Qu, J., Zhou, F., Song, J., and Shen, G. (2021). Recent Advances in Perovskite Photodetectors for Image Sensing. Small *17*, e2005606.
26. Hossain, A., Bandyopadhyay, P., Karmakar, A., Ullah, A.A., Manavalan, R.K., Sakthipandi, K., Alhokbany, N., Alshehri, S.M., and Ahmed, J. (2022). The hybrid halide perovskite: Synthesis strategies, fabrications, and modern applications. Ceram. Int. *48*, 7325–7343.
27. Li, G., Wang, Y., Huang, L., and Sun, W. (2022). Research Progress of High-Sensitivity Perovskite Photodetectors: A Review of Photodetectors: Noise, Structure, and Materials. ACS Appl. Electron. Mater. *4*, 1485–1505.
28. Xie, H., Pan, Q., Wu, D., Qin, F., Chen, S., Sun, W., Yang, X., Chen, S., Wu, T., Chi, J., et al. (2022). Lateral Heterostructured Vis-NIR Photodetectors with Multimodal Detection for Rapid and Precise Classification of Glioma. ACS Nano *16*, 16563–16573.
29. Xue, T., Huang, Z., Zhang, P., Su, M., Hu, X., Wu, T., Fan, B., Chen, G., Yu, G., Liu, W., et al. (2022). A shape memory scaffold for body temperature self repairing wearable perovskite solar cells with efficiency exceeding 21. InfoMat *4*, e12358.
30. Yu, R., Wu, G., Shi, R., Ma, Z., Dang, Q., Qing, Y., Zhang, C., Xu, K., and Tan, Z. (2022). Multidentate Coordination Induced Crystal Growth Regulation and Trap Passivation Enables over 24% Efficiency in Perovskite Solar Cells. Adv. Energy Mater. *13*, 2203127.
31. Pan, L., Li, H., Chang, B., and Yin, L. (2022). Crystallization and Defect Regulation in Sn–Pb Perovskite Solar Cells via Optimized Anti Solvent Passivation Strategy. Sol. RRL *6*, 2200398.
32. Li, J., Li, B., Yang, G., Zheng, D., and Yu, J. (2023). Crystallization and defects regulation of efficient inverted perovskite solar cells via glycine ethyl ester hydrochloride. Appl. Surf. Sci. *608*, 155269.
33. Zheng, X., Wu, C., Jha, S.K., Li, Z., Zhu, K., and Priya, S. (2016). Improved Phase Stability of Formamidinium Lead Triiodide Perovskite by Strain Relaxation. ACS Energy Lett. *1*, 1014–1020.
34. Kulbak, M., Gupta, S., Kedem, N., Levine, I., Bendikov, T., Hodes, G., and Cahen, D. (2016). Cesium Enhances Long-Term Stability of Lead Bromide Perovskite-Based Solar Cells. J. Phys. Chem. Lett. *7*, 167–172.
35. Gershon, T., Shin, B., Bojarczuk, N., Hopstaken, M., Mitzi, D.B., and Guha, S. (2015). The Role of Sodium as a Surfactant and Suppressor of Non-Radiative Recombination at Internal Surfaces in Cu_2ZnSnS_4. Adv. Energy Mater. *5*, 1400849.
36. Tong, Z., Yan, C., Su, Z., Zeng, F., Yang, J., Li, Y., Jiang, L., Lai, Y., and Liu, F. (2014). Effects of potassium doping on solution processed kesterite Cu_2ZnSnS_4 thin film solar cells. Appl. Phys. Lett. *105*, 223903.
37. Wang, Q., Lyu, M., Zhang, M., Yun, J.H., Chen, H., and Wang, L. (2015). Transition from the Tetragonal to Cubic Phase of Organohalide Perovskite: The Role of Chlorine in Crystal Formation of $CH_3NH_3PbI_3$ on TiO_2 Substrates. J. Phys. Chem. Lett. *6*, 4379–4384.
38. Lu, Z., Lou, Y., Xiao, L., Xu, X., Wang, C., Li, L., Su, X., and Zou, G. (2022). Grain Slip Derived Network Topology to Remarkable Strength–Toughness Combination of Perovskite Film for Flexible Solar Cells. Adv. Energy Mater. *12*, 2202298.
39. Li, Y., Chen, Z., Yu, B., Tan, S., Cui, Y., Wu, H., Luo, Y., Shi, J., Li, D., and Meng, Q. (2022). Efficient, stable formamidinium-cesium perovskite solar cells and minimodules

enabled by crystallization regulation. Joule *6*, 676–689.

40. Fu, S., Zhang, W., Li, X., Wan, L., Wu, Y., Chen, L., Liu, X., and Fang, J. (2020). Dual-Protection Strategy for High-Efficiency and Stable CsPbI2Br Inorganic Perovskite Solar Cells. ACS Energy Lett. *5*, 676–684.
41. Rao, L., Meng, X., Xiao, S., Xing, Z., Fu, Q., Wang, H., Gong, C., Hu, T., Hu, X., Guo, R., and Chen, Y. (2021). Wearable Tin-Based Perovskite Solar Cells Achieved by a Crystallographic Size Effect. Angew. Chem. Int. Ed. Engl. *60*, 14693–14700.
42. Hwang, T., Lee, B., Kim, J., Lee, S., Gil, B., Yun, A.J., and Park, B. (2018). From Nanostructural Evolution to Dynamic Interplay of Constituents: Perspectives for Perovskite Solar Cells. Adv. Mater. *30*, e1704208.
43. Hu, H., Singh, M., Wan, X., Tang, J., Chu, C.-W., and Li, G. (2020). Nucleation and crystal growth control for scalable solution-processed organic–inorganic hybrid perovskite solar cells. J. Mater. Chem. A *8*, 1578–1603.
44. Singh, R., Nazim, M., Kini, G.P., and Kan, Z. (2022). Perovskite Based Photovoltaics for Artificial Indoor Light Harvesting: A Critical Review. Sol. RRL *7*, 2200953.
45. Yan, B., Liu, X., Lu, W., Feng, M., Yan, H.-J., Li, Z., Liu, S., Wang, C., Hu, J.-S., and Xue, D.-J. (2022). Indoor photovoltaics awaken the world's first solar cells. Sci. Adv. *8*, eadc9923.
46. Wu, D., Xu, Y., Zhou, H., Feng, X., Zhang, J., Pan, X., Gao, Z., Wang, R., Ma, G., Tao, L., et al. (2022). Ultrasensitive, flexible perovskite nanowire photodetectors with long term stability exceeding 5000 h. InfoMat *4*, e12320.

STAR★METHODS

KEY RESOURCES TABLE

REAGENT or RESOURCE	SOURCE	IDENTIFIER
Chemicals, Peptides, and Recombinant Proteins		
MAI	Xi'an *p*-OLED	CAS: 14965-49-2
Lead (II) iodide (PbI_2)	Xi'an *p*-OLED	CAS: 10101-63-0
N, N-dimethylformamide (DMF)	Sigma-Aldrich	CAS: 68-12-2
Dimethyl sulfoxide (DMSO)	Sigma-Aldrich	CAS: 67-68-5
Chlorobenzene (CB)	Aladdin	CAS: 108-90-7
4-Acetamidothiophenol (AMTP)	Aladdin	CAS: 1126-81-4

RESOURCE AVAILABILITY

Lead contact

Further information and requests for resources and reagents should be directed to and will be fulfilled by the lead contact, Meng Su (sumeng1988@iccas.ac.cn).

Materials availability

This study did not generate new unique reagents.

Data and code availability

- Data: All data reported in this paper will be shared by the lead contact upon request.
- Code: This paper does not report original code.
- Any additional information required to reanalyze the data reported in this paper is available from the lead contact upon request.

EXPERIMENTAL MODEL AND SUBJECT DETAILS

This work did not need any unique experimental model.

METHOD DETAILS

Experimental procedures

Solution preparation

214.65 mg MAI and 622.35 mg PbI_2 were dissolved in a mixed solvent of 900 μL DMF and 100 μL DMSO. The above solution was sealed and stirred on a hot table at 55°C for 2 h to obtain the methylammonium lead lodide ($MAPbI_3$) solution. 5 mg AMTP was dissolved in 1 mL DMSO and then stirred on a hot table at 60°C for 2 h to prepare the AMTP solution. AMTP solutions of 16, 32 and 48 μL were added to $MAPbI_3$ solution respectively to obtain AMTP- $MAPbI_3$ mixed solution of 0.01wt %, 0.02wt % and 0.03wt %. The mixed solution was heated on a hot stage at 60°C and stirred for 2 h to fully mix the AMTP molecules with $MAPbI_3$ precursor solution to obtain AMTP doped $MAPbI_3$ solution.

Fabrication of the detector substrate

A 1.5 × 1.5 cm^2 cross finger electrode was fabricated on the polyimide (PI) film by an etching process. Select a 2 × 2 cm^2 glass substrate, wipe it gently with alcohol, and blow dry with nitrogen gas. 300 μL polydimethylsiloxane (PDMS) were dripped onto the treated glass substrate and rotated for 30 s at a rotational speed of 2000 rpm to obtain evenly spread PDMS film. The PI film with a gold electrode was gently attached to the surface of the wet PDMS, and was heated on a hot table at 80°C for 4 h. When the PDMS fully solidified, the detector substrate was completed.

Preparation of the detector

40 μL of AMTP-doped perovskite precursor solution was dropped onto the detector substrate then was spin-coated at 4000 rpm for 30 s. 250 μL of anti-solvent chlorobenzene was added after 7 s of the spin coating process. Subsequently, the prepared wet film was heated at 100°C for 10 min to obtain AMTP-$MAPbI_3$ film. 200 μL PDMS was dripped onto AMTP-$MAPbI_3$ film and spun at 2000 rpm for 30 s as the encapsulation layer. Finally, the sample was heated on a hot table at 60°C for 2 h. The AMTP-$MAPbI_3$ based photodetector was obtained by peeling the PI base from the glass plate with a blade.

Film characterizations

The morphology of films was measured by SEM (HITACHI, S-4800, Japan) at an accelerating voltage of 5.0 kV. The ultraviolet-visible (UV-Vis) spectra were recorded by SHIMADZU, UV-2600. The photoluminescence (PL) spectra and time-resolved photoluminescence (TRPL) spectra at the peak emission of 650–900 nm were measured by photoluminescence spectroscopy (Edinburgh Instruments Ltd., FLS980).

Detector characterizations

The current-time (I-T) curves and current-voltage (I-V) curves were characterized by a semiconductor tester (Keithley, 4200A-SCS). The light intensity was measured by an illuminometer (Deli, DL333204). The flashlight (SKYFIRE, SF-656S) provided white light source.